# Fast Acquisition Tunable High-Resolution Photon-Counting OTDR

Calliari, Felipe; Correia, Marlon M.; Temporao, Guilherme Penello; Amaral, Gustavo C.; Weid, Jean Pierre Von Der

**DOI**
10.1109/JLT.2020.2990872

**Publication date**
2020

**Document Version**
Accepted author manuscript

**Published in**
Journal of Lightwave Technology

**Citation (APA)**
Calliari, F., Correia, M. M., Temporao, G. P., Amaral, G. C., & Weid, J. P. V. D. (2020). Fast Acquisition Tunable High-Resolution Photon-Counting OTDR. *Journal of Lightwave Technology*, *38*(16), 4572-4579. Article 9079665. https://doi.org/10.1109/JLT.2020.2990872

# Fast Acquisition Tunable High-Resolution Photon-Counting OTDR

Felipe Calliari, Marlon M. Correia, Guilherme Penello Temporão, Gustavo C. Amaral *Member, IEEE*, and Jean Pierre von der Weid *Senior Member, IEEE*

***Abstract*—A 15 dB dynamic range and 4.6 cm spatial resolution tunable photon-counting optical time-domain reflectometer (PC-OTDR) is presented along with a Field Programmable Gate Array (FPGA)-based detection management system that allows several regions of the fiber to be interrogated by the same optical pulse, increasing the data acquisition rate when compared to previous solutions. The optical pulse generation is implemented by a tunable figure-8 passive mode-locked laser providing pulses with the desired bandwidth and center wavelength for WDM applications in the C-band. The acquisition rate is limited by the afterpulse effect and dead time of the employed gated avalanche single-photon detectors. The devised acquisition system not only allows for centimeter-resolution monitoring of fiber links as long as 12 km in under 20 minutes but is also readily adapted to any other photon-counting strategy for increased acquisition rate. The system provides a 20-fold decrease in acquisition times when compared with state-of-the-art solutions, allowing affordable times in centimeter-resolution long-distance fiber measurements.**

***Index Terms*—Optical fiber monitoring; optical time domain reflectometry; single-photon detection.**

## I. Introduction

OPTICAL FIBERS are, inarguably, one of the most important elements of modern telecommunication networks, having allowed for long-haul high-bandwidth links to be implemented around the world [1]. They offer, thus, the basis for the Open Systems Interconnection (OSI) and its reliability is fundamental for the robust operation of all the higher-level network layers. Mechanical damage, the protagonist of optical fiber transmission impairments, can cause from minor to debilitating losses and, therefore, must be evaluated timely and precisely [2].

One way of discovering the position and magnitude of the mechanical damage imposed into a fiber is to monitor the back-propagating light originated from an interrogation signal; the nature of such light falls into two classes: scattered light, usually associated with the Rayleigh backscattering of light from the atomic nuclei of the fiber material; and reflected light, usually associated with the discontinuity of index of refraction along the fiber or to a reflective structure placed along the fiber, such as a Bragg grating; the last of which figures as the basis of several of the proposed and implemented distributed fiber sensors [3].

When the intensity of the back-propagating light is measured over time, and the position of the mechanical damage is determined based on the speed of light inside the fiber, the method is known as Optical Time Domain Reflectometry (OTDR) [4]. In OTDR applications, spatial resolution and dynamic range come as a trade-off since strengthening the pulse for enhanced reach usually affects the pulse width and diminishes the 2-point resolution [5]. To alleviate such trade-off, a photon-counting OTDR (PC-OTDR) can be assembled, where a single-photon detector is employed and a detection management system must be integrated for consistent results [6]. In recent works [7], [8], PC-OTDR systems have been developed where a train of detection gates allows for several positions of the fiber to be interrogated with a single optical pulse. Employing the same mechanism in systems with centimeter-range resolutions, which can benefit both optical fiber monitoring and sensor applications, has been elusive. In [9], for instance, a system making use of two different PC-OTDR variants was demonstrated in order to achieve centimeter-range resolution in km-range fibers without the drawback of low data acquisition rate imposed by the high-resolution acquisition procedure. There, extra signal processing steps had to be taken into account, which reduced the total monitoring speed.

In this work, a 15 dB dynamic range and 4.6 cm spatial resolution tunable photon-counting optical time-domain reflectometer (PC-OTDR) is presented along with a joint Field Programmable Gate Array (FPGA) and Time-to-Digital Converter (TDC)-based detection management system that allows several regions of the fiber to be interrogated by the same optical pulse. The optical pulse generation is implemented by a figure-8 passively mode-locked laser containing a tunable optical filter that ensures that the probing pulses are generated within the desired bandwidth and center wavelength for WDM applications. The developed detection procedure allows for increasing the data acquisition rate by a factor that depends on the operator's choice of detection window length and detection gate train period. The results indicate that portions of the fiber separated by 200 meters can be interrogated by the same optical pulse without debilitating effects coming from the afterpulse effect. Centimeter-range monitoring of km-range fibers in under 20 minutes in a wavelength division

F. Calliari, M. M. Correia, G. P. Temporão, and J. P. von der Weid are with the Center for Telecommunications Studies, Pontifical Catholic University of Rio de Janeiro, RJ, Brazil (e-mail: {felipe.calliari,mcorreia,temporao,vdweid}@opto.cetuc.puc-rio.br).

G. C. Amaral is with the Center for Telecommunications Studies, Pontifical Catholic University of Rio de Janeiro, RJ, Brazil and with the QC2DLab, Kavli Foundation, Technical University of Delft, The Netherlands (e-mail: gustavo@opto.cetuc.puc-rio.br).

multiplexing (WDM) scenario are demonstrated in this paper.

The paper is divided as follows. The architecture and its sub-systems are presented in Section II, where the arrangement of the devices, individual characteristics, and data management are presented and discussed. Section III approaches the characteristics of the full system with respect to its achievable spatial resolution and dynamic range, tunability, acquisition rate, and limitations on such. Section IV provides discussion on possible applications and optimizations of the system and concludes with the major contributions and future works.

## II. Architecture

The basic operation of a PC-OTDR begins with the optical pulse generation sub-system, which creates light pulses at a rate such that only one pulse traverses the fiber at a time. Under this condition, back-propagating light created due to either scattering or reflection of the interrogation pulse can be collected by means of an optical circulator and sent to a single-photon detector. It is the task of the data acquisition sub-system to correctly associate detections to time windows such that, with an estimate of the fiber's refractive index and the speed of light, one can determine the positions where the back-propagating signals are originated. In mathematical form, $d_i = \frac{c}{2\,n}\,t_i$, where $c$ is the speed of light in vacuum, $n$ is the refractive index of the fiber and $t_i$ is the round-trip travel time of the i-th detected pulse, taken into account by the factor 2 in the denominator.

In order to simplify the analysis of the OTDR signal, one can ignore the non-linear effects associated to the transmission of optical signals, which allow the employment of linear system abstractions such as the transfer function and the impulse response. In this context, and since the optical fiber is a two-port network, the OTDR procures to measure the impulse response $h\,(t)$ of the fiber's $S_{11}$ parameter, or $h_{11}\,(t)$; in fact, optical frequency-domain reflectometry (OFDR) techniques [10] such as the Incoherent- and Coherent-OFDR attempt to assess the transfer function $H_{11}\,(f)$ of the fiber, which is intimately related to $h_{11}\,(t)$ via a Fourier transform. Due to the intrinsic attenuation of light inside an optical fiber, $h_{11}\,(t)$, which, when translated into distance is usually referred to as the fiber profile, exhibits an exponential decay; it is, thus, usual to display the fiber profile in logarithmic scale with a linear negative slope, where eventual breaks can be associated to power losses [11], [12].

It becomes clear that the spatial resolution achievable in the measurement of the fiber profile is limited by the temporal width of the interrogating pulse, $p\,(t)$, since

$$h_{11}^{\text{eff}}\,(t) = h_{11}\,(t) * p\,(t)\,, \tag{1}$$

where $h_{11}^{\text{eff}}\,(t)$ stands for the effectively measured fiber profile. At the same time, the overall energy contained in $p\,(t)$ will determine the amount of attenuation that it can withold while still allowing for a higher-than-one signal-to-noise ratio (SNR $> 1$) measurement in the detector. Assuming saturation of the optical pulse generation structure, in order to increase the optical energy contained in the probing pulse, its width must be increased, thereby constituting the so-called trade-off between spatial resolution and dynamic range. Attempting to extract the maximum of both ends of this trade-off, one can employ sources of high-power narrow optical pulses and low noise-equivalent power (NEP) detectors. Moreover, management and synchronization of pulse generation and data acquisition is imperative for efficient long-reach high-resolution measurement. In the following sub-sections, these two sub-systems (optical pulse generation and data acquisition) are presented in detail.

### A. Optical Pulse Generation

The optical pulse generation sub-system is comprised of a figure-eight passively mode-locked laser (F8-PMLL). Such laser configuration has been shown to produce sub-picosecond pulses at different wavelengths [13], rendering its application for a tunable, long-reach, high-resolution time-domain reflectometer. Mode-locked lasers rely on saturable absorbers to create a fixed phase relation between the spectral modes allowed within its optical resonator cavity. Under the mode-locked condition, the temporal shape of the output signal is given by a coherent weighted sum of such allowed spectral modes or, mathematically:

$$p\,(t) = \sum_{n=-N/2}^{N/2} c_n e^{-i2\pi(\omega_0 + n\cdot f_0)t}, \tag{2}$$

where $c_n$ are the individual weigths of each spectral modes (or Fourier coefficients), $\omega_0$ is the laser's center frequency, $f_0$ is the optical cavity's free-spectral range (FSR), and $N$ is the total number of allowed spectral modes within the laser bandwidth $\Delta\omega$, where $N = \Delta\omega / f_0$. Equation 2 states that the cavity modes constitue a Fourier series of the output signal, which will correspond to periodically emitted pulses since the spectrum, during mode-locked operation, takes the form of a frequency comb.

Mode-locking can be achieved either actively (through intensity and/or phase modulation) or passively in either free-space or fiber cavities [14]. Among others, the main advantages of fiber-based mode-locked lasers include low propagation loss, the possibility of creating high Q value kilometer-long fiber cavities, and the fact that erbium-doped fiber amplifiers (EDFAs) and fiber-pigtailed semiconductor optical amplifiers (SOAs) can be used as the gain media [14]. Figuring as physical mechanisms that guarantee mode-locking in PML fiber lasers are nonlinear polarization rotation [15], dispersion-managed stretched pulse propagation [16], and the constructive/destructive interference of counter-propagating longitudinal modes in a so-called nonlinear amplifying loop mirror (NALM) [17]. The latter allows for the optical switching of the input optical pulses according to the following mathematical relations:

$$\begin{aligned} \mathcal{T} &= \tfrac{I_{\text{out}}}{I_{\text{in}}} = \tfrac{\mathrm{G}(1-\cos[\Delta\phi_{\text{NL}}(\mathrm{G}-1)])}{2} \\ \mathcal{R} &= 1 - \mathcal{T}, \end{aligned} \tag{3}$$

where $I_{\text{in/out}}$ are the input/output optical intensities, G is the amplifier gain, $\Delta\phi_{\text{NL}}$ is the difference in non-linear phase shift between the counter-propagating fields in the NALM, and $\mathcal{T}$ and $\mathcal{R}$ are the transmissivity and reflectivity of the NALM, respectively.

When the NALM is combined with a closed fiber loop, it constitutes a figure-8 laser (F8L), an extremely versatile fiber structure that finds applications in, for instance, soliton generation, and has been first reported by Duling [18]. Recently, an F8L realized with an SOA in the NALM and an EDFA in the optical cavity has been reported [19], whose design is reproduced in this work and depicted in Fig. 1. The NALM (left-hand side in Fig. 1) is composed by an SOA, a Polarization Controller (PC), and single-mode fibers totalling a length of $L_1 \approx 8.42$ meters. The optical cavity (right-hand side in Fig. 1) is formed by a PC, a 90/10 coupler (that allows one to couple a portion of the optical signal generated in the F8L to the output), a tunable band pass filter (BPF),an unidirectional EDFA (incorporating an optical isolator), and single-mode fibers totaling a length of $L_2 \approx 36.38$ meters.

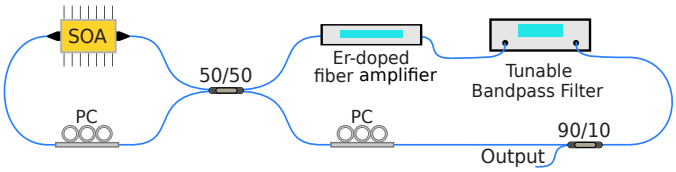


Fig. 1. The overview of the passively mode-locked figure-8 fiber laser. On the left-hand side, the nonlinear amplifying loop mirror (NALM) is depicted. On the right-hand side, the optical cavity with an unidirectional EDFA that determines the direction of propagation, and a variable optical bandpass filter that determines the center wavelength of emission are depicted. PC, Polarization Controller.

In the NALM, a periodic transmission and reflection of the optical pulses occurs as a function of the instantaneous input power and the non-linear phase shift between the longitudinal counter-propagating modes supported by the NALM cavity. Therefore, if an optical pulse is formed in the F8-PMLL and its peak power satisfies the transmission conditions of the NALM, it will propagate in the F8-PMLL according to the direction dictated by the optical isolator; otherwise, it will be reflected by the NALM and eliminated by the EDFA's isolator [20]. The polarization controller of the left-hand side loop (1) can be adjusted to control the birefringence in the fiber and, in turn, the non-linear phase shift factor in Eq. 3. This way, the interference of the counter-propagating longitudinal modes on the 50/50 coupler can be adjusted such that only input pulses of a certain intensity are transmitted, while lower pulses are reflected and extinguished in the EDFA's isolator. The center wavelength of emission of the F8L is dictated by the BPF, which is tunable in the range 1530 - 1565 nm covering the telecommunication C-band as depicted in Fig. 2.

Under fundamental mode operation, the F8-PMLL presented in Fig. 1 produces 303 ps-wide pulses spaced by 224 ns (a repetition rate of 4.46 MHz), the former determined by a total 1.39 GHz emission bandwidth and, the latter, by the overall length of the fiber cavity of 44.8 meters. To achieve such conditions, other than correctly adjusting the PCs, the injection current of the SOA should be approximately 150 mA, which translates into optical pulses with 4 pJ energy level and 13 mW peak power. Under these conditions, the wavelength tunability of the F8-PMLL is rather simple in terms of PC alignment; on the other hand, the pulse peak power limits the achievable dynamic range. In order to maintain the ease of

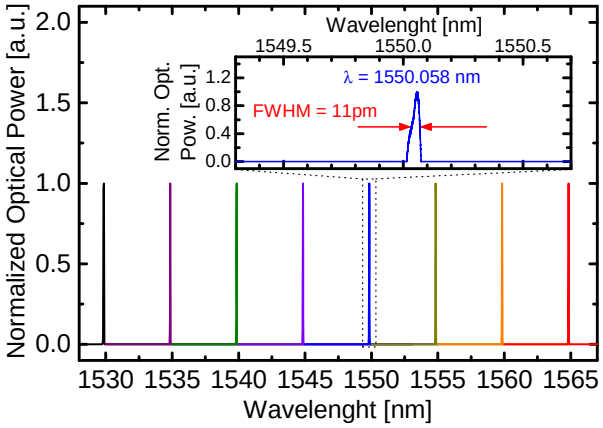


Fig. 2. Center wavelength tunability of the employed F8-PMLL. The bandwidth, measured with a high-resolution (16 MHz) optical spectrum analyzer, is 11 pm at all center wavelengths.

tunability of the system while also increasing the dynamic range, the output pulses were sent to a second EDFA, which yields optical pulses with 25 pJ energy level and 83 mW peak power. Due to the broad bandwidth of the EDFA, the width of the optical pulses, after amplification, was not compromised, as presented in Fig. 3; the output spectrum, measured in a electrical spectrum analyzer (ESA), corroborates the timing characteristics of the optical signal, and is presented in Fig. 4.

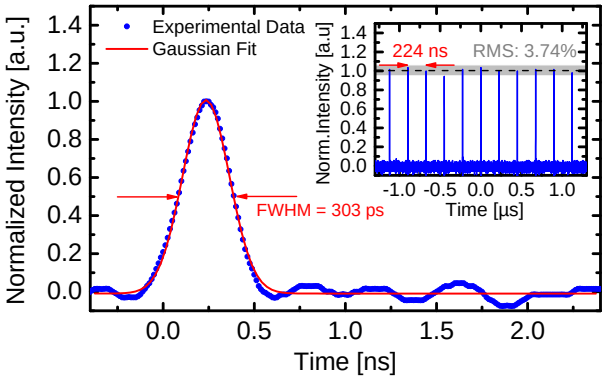


Fig. 3. Temporal shape of the generated optical signal in the passive mode-locked figure-8 laser. The pulse separation of 224 ns matches the resonator length of 44.8 meters and the pulse temporal width is 303 ps, which limits the spatial resolution of the PC-OTDR to 3.07 cm.

### *B. Data Acquisition*

Data acquisition is performed in synchronization with an enabling pulse from a high-speed optical switch that guarantees that a single probing pulse is traversing the fiber at a time. This is necessary since the rate of pulse emission from the PML described in the previous subsection (which is entirely determined by the cavity length of the optical resonator) might not match this condition. The pulse selection is accomplished through an SOA triggered by a short (2 ns, 300 mA) pulse, which, under these conditions, imparts a 1 dB insertion loss on the optical pulse and creates an ASE noise level of -9.6 dBm, setting the probing pulse's extinction ratio to 27 dB.

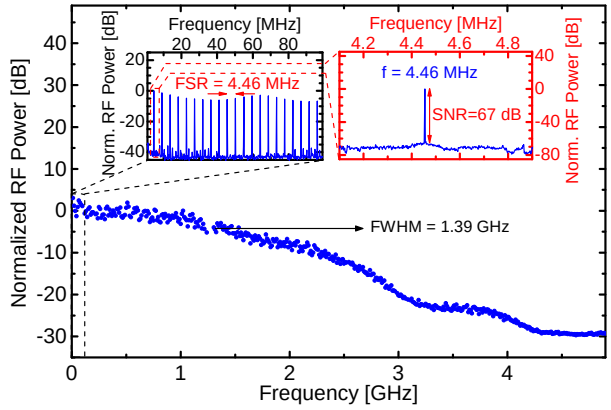


Fig. 4. Spectral characterization of the generated optical signal with respect to the central wavelength of 1550.058 nm. The spectral comb-shape exhibits a finesse $\mathcal{F} = 6371.43$, with a bandwidth ($\delta f$) of 700 Hz and a free-spectral range (FSR) of 4.46 MHz, which matches the resonator length of 44.8 meters.

This triggering pulse, in turn, is synchronized to the incoming pulse from the PML by detecting a small portion of its output using a 90/10 beam splitter.

The block diagram of the data acquisition sub-system is depicted in Fig. 5. Synchronization is crucial not only between the PML and the SOA but, also, between these and a Field Programmable Gate Array (FPGA), a Time-to-Digital Converter (TDC), and the single-photon detector that manage the detection of the backscattered portion of the probe pulse. A Digital Delay Generator ($DDG_1$), triggered by detections from the F8-PMLL pulses, is responsible for reducing the rate of pulses launched into the fiber by means of an internal prescaler. It is also responsible for generating a delayed trigger ($\tau_p$) for a second DDG ($DDG_2$) that works in burst mode; the importance of $\tau_p$ will be clarified further on. $DDG_2$ then generates a sequence of evenly-spaced ($\tau_b$) electrical pulses that act on the TDC as a *start* pulse and are also routed to the FPGA. The FPGA is programmed such that the pulse received by $DDG_2$ goes through an AND gate and is enabled according to a pre-defined signal $e_r$, whose function will also be clarified further on; presently, $e_r$ is considered always high, for simplicity.

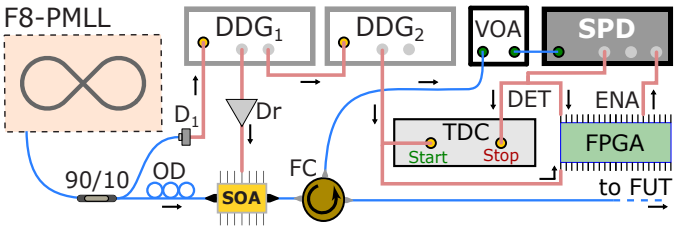


Fig. 5. Block diagram of the data acquisition system including the synchronization with the F8-MPLL; optical fibers are blue lines and pink lines are electrical signals. $D_1$, *p-i-n* photodetector; Dr, electronic driver; OD, optical delay; FC, fiber circulator; VOA, variable optical attenuator; FUT, fiber under test. The black arrows indicate the direction of the electric and optical signals for ease of visualization.

The output of the FPGA's AND gate is directed to the enable input of the SPD, opening a detection window ($\tau_d$) whose width can be tuned between 5 and 35 ns. If a detection occurs within this detection window, the detection pulse of the SPD is directed to the *stop* input of the TDC where the time difference between *start* and *stop* pulses is determined. The detection pulse is also sent to the FPGA, that records the occurrence of a detection. In case no detection occurs, the subsequent pulse from $DDG_2$ will reinitialize the process and the FPGA will record the absence of a detection in the previous detection window. The FPGA can, then, produce a simple binary indexed list to backtrack the detection events: 1's correspond to the occurrence of a detection; and 0's to no detection.

The fact that the system is able to reinitialize the data acquisition every new cycle of the burst of $DDG_2$ allows a single optical pulse to probe regions of the fiber spaced by $d = \frac{c}{2n}\tau_b$. In order to reconstruct the fiber profile, one is required to measure the time between the pulse being launched into the fiber and any of the *stop* pulses, which can be accomplished by combining the information from the FPGA and the TDC. This is due to the TDC's data storage procedure, which piles up the time between the *start* and *stop* pulses only when a corresponding *stop* occurs; the FPGA provides, thus, a means of associating the times in the TDC to the correct detection windows which produced them. Furthermore, since $\tau_p$ represents an offset in time between the probing pulse being launched into the fiber and the opening of the detection windows, it must also be taken into account in order to write any detection time as:

$$\tau_{\text{det}} = \tau_p + i\tau_b + \tau^i_{\text{TDC}}, \tag{4}$$

where $i$ corresponds to the index of the respective enabling pulse of $DDG_2$ in which a detection was recorded and $\tau_{\text{TDC}}$ is the time stored in the TDC after a detection.

Clearly, in order to probe all the points in the fiber, $\tau_p$ must be swept so that it covers the distance between two consecutive detection windows. The total number of steps for $\tau_p$ can then be calculated according to $\frac{\tau_b}{\tau_d}$ and has a direct impact on the total measurement time, as will be discussed in the next section. In order to clarify the whole procedure, Fig. 6 depicts, in (a), the time panels of all the relevant optical and electrical signals associated to the data acquisition subsystem. In (b), the event lists contained within the FPGA and the TDC are pictorially depicted as well as the procedure for combining the two lists and create the fiber profile.

## III. The Fast Acquisition Tunable High-Resolution PC-OTDR

Combining the previously described sub-systems culminates in an optical reflectometry-based measurement system that yields a spatial resolution in the centimeter range with both achievable dynamic range and data acquisition rates higher than related state-of-the-art systems; furthermore, the system is tunable around the telecommunication C-band and exhibits narrow bandwidth, making it ideal for supervision of currently deployed optical networks relying on wavelength division multiplexing (WDM), such as WDM Passive Optical Networks (WDM-PON).

In order to characterize the system's operation parameters, OTDR profiles of different fibers have been measured; depending on the figure of merit of interest, the condition of

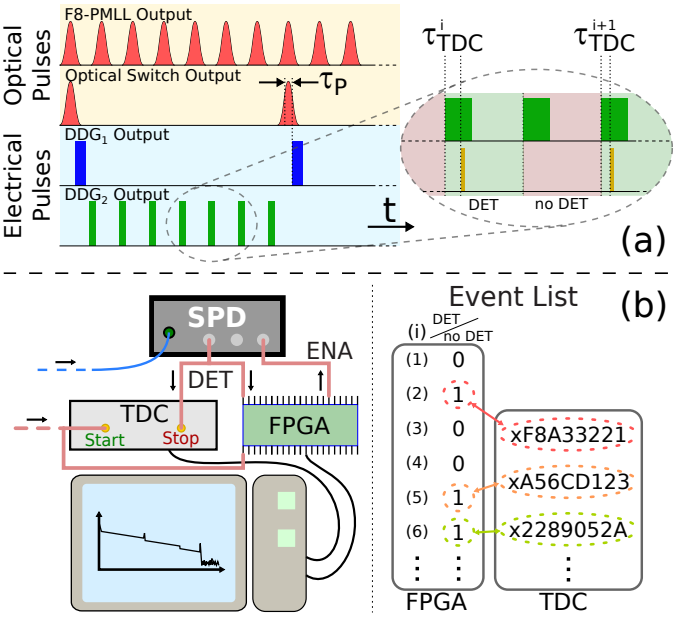


Fig. 6. Data acquisition subsystem procedure. (a) Time panel of relevant electrical and optical pulses. The zoomed region represents two different situations, i.e., detection windows with and without an associated detection pulse. Furthermore, the time between the enabling of the detector and the arrival of the detection pulse (different for the two depicted events) is recorded by the TDC as $\tau_{\text{TDC}}$. (b) The detection system for reconstruction of the fiber profile based on the event lists from the FPGA and the TDC. On the left hand side, the connections between the devices is depicted as a block diagram including a personal computer; optical fibers are blue lines, pink lines are electrical signals, and black lines are data buses. The right hand side depicts the combination of the results from the event lists that allow for the reconstruction of $\tau_{\text{det}}$.

the measurement also changed. This is because, even with the higher data acquisition rates propitiated by the proposed system, measurements of km-long fibers that achieve the full dynamic range of the system still require long measuring times. In Fig. 7, for instance, the dynamic range and spatial resolution are showcased using a 8-km fiber; only the measurements of detection windows associated to a fixed $\tau_p$ were acquired, however, but during an extended 5-min measurement time ($t_{\text{meas}}$).

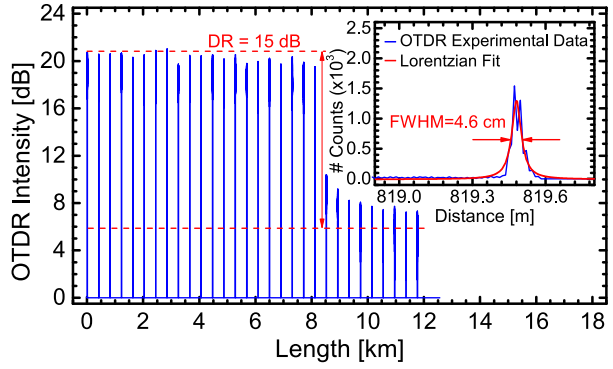


Fig. 7. Dynamic range (15 dB) and spatial resolution (4.6 cm) achieved with the proposed OTDR system. The wavelength of operation of the F8-PMLL for these results was 1550.058 nm, and the total measurement time was 5 minutes.

For this measurement, a detection window $\tau_d = 20$ ns and a burst period $\tau_b = 2$ $\mu$s were used, yielding a 15 dB dynamic range, calculated by taking the difference, in dB, between the initial point of the profile and the 1.5-dB point below the noise level (which coincides with the average value of the noise) [21], i.e., detections associated to positions "outside" the fiber. The value of the dynamic range agrees well with the prediction based on the mean number of photons per detection window at the initial position of the fiber (0.45), the rate of emission of probing pulses into the fiber (9 KHz), and the dark count rate of the detector (5 per second). The VOA at the input of the SPD guarantees that the mean number of photons impinging on the SPD is such that multi-photon detection is reduced so that the OTDR trace exhibits no saturation effects [8]. The VOA attenuation is set to $\sim 15$ dB, calculated based on the pulse peak power at the input of the fiber, the photon's energy, and the Rayleigh scattering coefficient. Under these conditions, the rate difference between detections (4100 per second) and dark counts equates to 14.5 dB, a good estimate of the achieved dynamic range in Fig. 7. The SPD operates at an efficiency of 5%, and the counting rate is 180,000 per second.

The total amount of time necessary to reproduce the results with the same dynamic range, but for all points in the fiber, would be $\frac{\tau_b}{\tau_d} t_{\text{meas}} \approx 8$ hours, which is the reason why these were not measured. The spatial resolution was determined by the full width at half maximum of a lorentzian fit onto a reflection peak at the fiber's end to be 4.6 cm as shown in the inset of Fig. 7. This value, which differs from the limit induced by the temporal width of the probing pulse, is attributed, mainly, to the jitter of the SPD, although the jitter associated to F8PMLL and to both the TDC and DDG also contribute. These values have been experimentally determined to be 350 ps, 20 ps, 40 ps, and 45 ps, respectively, which, combined with the pulse width, amount to a spatial resolution of 4.9 cm, which agrees well with the experimentally determined values.

In order to showcase the capability of the system to perform tunable and fast fiber profile measurements with centimeter resolution, an arrayed waveguide grating (AWG) was employed. A 4-km feeder fiber (between the measurement system and the AWG) is followed by four different fibers ($L_1$ = 4 km, $L_2$ = 8 km, $L_3$ = 0.9 km, $L_4$ = 3 km) each connected to a different channel of the AWG, as follows: Ch 03, $\lambda$ = 1534.09 nm, $L_1$; Ch 09, $\lambda$ = 1539.8 nm, $L_2$; Ch 15, $\lambda$ = 1544.0 nm, $L_3$; Ch 22, $\lambda$ = 1550.0 nm, $L_4$. For these results, the measurement time for each of the values of $\tau_p$ was set to ten seconds, and the number of total steps necessary in order to cover all the points in the fiber was $\frac{\tau_b}{\tau_d} = \frac{2\mu s}{20\text{ns}} = 100$, totalizing a measurement time of $\sim$16.7 minutes. Interrogation of each individual channel is possible by tuning the F8-PMLL center wavelength accordingly, and the results are presented in Fig. 8.

Under these conditions, the amount of detection events are still not enough to reach the full dynamic range of the system, as previously commented, and as clearly depicted in the traces of Fig. 8. Even under such short measurement time conditions, however, the system was able to achieve a quite expressive $\sim$12 dB dynamic range. Furthermore, the system showcases tunable centimeter-resolution measurements

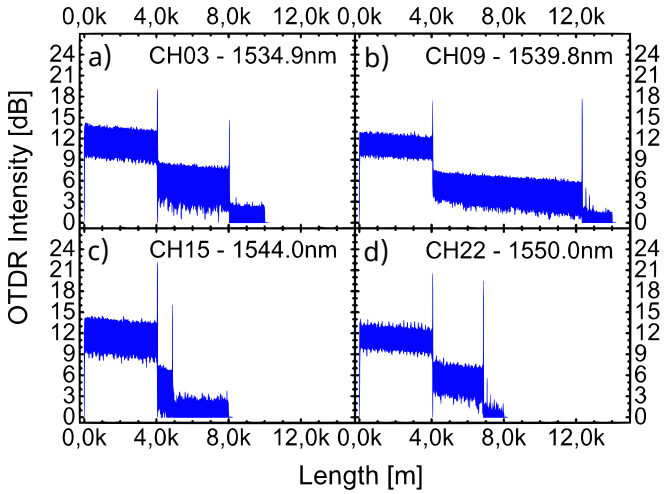


Fig. 8. Full fiber measurements of four distinct AWG channels, corresponding to different wavelengths. The tunability of the F8-PMLL allows for each channel to be probed individually. Total measurement time is ∼16.7 minutes for each of the channels. Detection peaks observed at the end of the fiber profiles correspond to afterpulsing due to the high reflection peak at the fiber end.

of km-range fibers in minute-range times, an outstanding result in comparison with state-of-the-art systems. Due to its performance, the system is dubbed the Fast Acquisition High-Resolution Photon Counting OTDR.

### A. Acquisition Rate and Afterpulse Probability

It is noteworthy that the burst period $\tau_b$ determines the speed-up in data acquisition of the proposed system, since a single optical probing pulse sent into the fiber can be used to interrogate multiple regions. Enabling more detection windows per optical pulse, which corresponds to decreasing $\tau_b$, even though positive in the sense of higher data acquisition rate, has an associated effect related to the afterpulse probability of the employed gated avalanche single-photon detectors. As the effective detector *deadtime* between two detection windows is reduced, the probability of a delayed release of a trapped carrier inside the semiconductor junction increases exponentialy [22].

For regions of the fiber where the counts associated to Rayleigh backscattered photons is above the noise (coming either from the intrinsic dark count rate of the detector of from the afterpulsing probability), the effect is not apparent; however, when one analyzes the detections outside of the fiber, where only the detector's intrinsic noise (dark count rate) should play a role, the effect becomes clear, as in positions $L \geq 8.2$ km of Fig. 7. In fact, if the separation between detection windows is too small, one can extrapolate the impact of the afterpulsing effect and expect that it completely degrades the measured OTDR profile, erasing all relevant information about the fiber.

Analyzing the impact of the afterpulse probability on the detections permits finding a set of parameters compatible with the sought after higher data acquisition rates while still minimizing as much as possible its contribution. Experimental results are presented in Fig. 9, where the difference, in dB, between the intrinsic noise level of the system, associated to the detector's dark count rate, and the noise level when the afterpulse is present, has been used as a figure of merit when the detection window length $\tau_d$ and the burst period $\tau_b$ are varied. In order to provide more insight into the results, the horizontal axis is presented in both $\mu$s and in meters, i.e., the associated distance separation, in the fiber, between two consecutive detection windows.

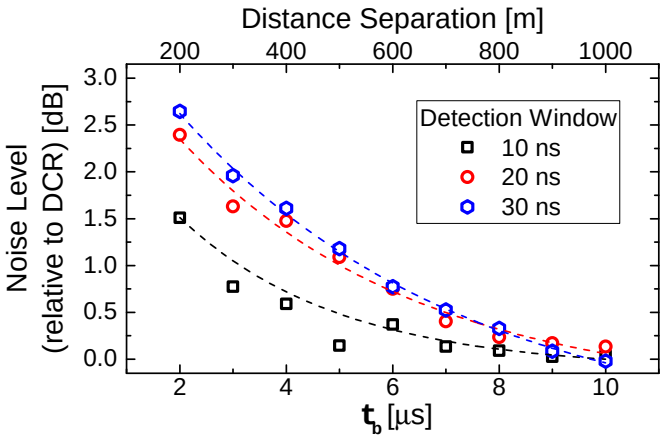


Fig. 9. Noise level, in dB, relative to the SPD's intrinsic dark count rate as the separation between detection windows and the width of such windows is varied. The exponential decay is expected from the behavior of the afterpulse probability as a function of *deadtime* [23].

As can be clearly seen from Fig. 9, the afterpulse probability dominates the noise baseline level unless the separation between consecutive detection windows is longer than 1 km. Simultaneously, the number of necessary windows $\frac{\tau_b}{\tau_d}$ for complete fiber measurements increases by a factor of 5, under thse conditions, with respect to the measurements of Fig. 8. Therefore, and since the impact of the afterpulse is not as critical on the noise level as the impact of increasing $\tau_b$ is on the timing, the parameters used in the measurement could be loosely selected as $\tau_b = 2$ $\mu$s and $\tau_d = 20$ ns.

### B. Discussion

It is clear that one of the major benefits of the proposed system is the capability of monitoring wavelength multiplexed networks with telecom-compatible wavelengths, which is available due to the tunability of the F8-PMLL. However, short-distance high-capacity optical networks operating at the near-infrared region of the spectrum are attracting a lot of attention [24], and high-resolution monitoring is of great interest in this context. In fact, a photon-counting OTDR system operating at this wavelength and making use of a gain-switched laser was recently demonstrated [25]. There, the acquisition rate is still limited since, for each probing pulse launched into the fiber, only a single detection window is enabled. Fortunately, the herewith proposed acquisition system can be readily adapted to work in that and any other photon-counting OTDR system with equal or even higher gains, since the silicon-based single-photon detectors compatible with that system exhibit lower dark count rates, higher detection efficiency, and smaller afterpulse probability. Systems such as

the one in [26], where a superconducting nanowire single-photon detector compatible with the telecom wavelength was employed in a PC-OTDR, or the one in [27], where a 30-dB dynamic range was achieved but with a total monitoring time of 6 hours, would likewise benefit from the proposed acquisition system.

It is noteworthy that the solution found in [9] to achieve cm-resolution fault detection at long-distances would also benefit from the high-rate acquisition system. There, a *coarse* and long-reach PC-OTDR system first acquires information about the fiber profile, which is followed by a signal processing routine that identifies possible candidates that are, then, individually interrogated by a *fine* PC-OTDR system. The limitation on the acquisition system, however, causes the total monitoring time to scale with the number of identified candidates, which is overcome with the current acquisition system, since multiple fault candidates can be interrogated simultaneously.

On one hand, thus, the acquisition system proposed and demonstrated in this work enables the high-resolution monitoring of long-distance fibers by greatly increasing the rate of data acquisition. On the other, the much higher event detection rate on the SPAD uncovers an application bottleneck associated to the maximum data capacity of the employed TDC. The fact that the current TDC is limited to 180 thousand samples per second caused the detection efficiency to be reduced to 5% in order to avoid loss of data; for higher values of detection efficiency the detection rate overloads the TDC. Employing a TDC with higher data capacity will allow for even higher data acquisition gains and could usher the replacement of the current avalanche single-photon detectors by superconducting nanowire single-photon detectors (SNSPD) that offer not only higher detection efficiency but also free-running operation.

The gain in speed over other centimeter-resolution PC-OTDR solutions is determined by the number of extra detection windows that the proposed system is capable of offering. Since this number will change if the fiber length increases and can also be leveraged against an increased contribution of the afterpulse effect (as shown in Figure 9), this number is hardly determined. For the measurement conditions showcased in Figure 7, however, 20 detection windows (within the fiber span) are available, which translates into a 20-fold factor in acquisition time in comparison with state-of-the-art solutions where only a single detection window is opened per optical pulse sent into the fiber [9], [25]. For the results of Figure 8, because the length of the fiber changes, the timing gain for the full-fiber measurement would vary between 10 and 20 using the current (limiting) devices and a reduced efficiency of the SPD. State-of-the-art (Superconducting Nanowire) Single-Photon Detectors offer absence of afterpulsing, higher than 90% detection efficiency, and as high as 100 ns deadtimes with 100 ps jitter. Allied to high-speed TDC modules, the system could perform the measurements showcased in Figures 7 and 8 in under a minute with higher resolution (due to the reduced jitter) and higher dynamic range (due to the absence of afterpulsing).

When compared to other monitoring solutions, which do not rely on photon-counting for fiber monitoring, the Fast Acquisition Tunable PC-OTDR exhibits an unique combination of characteristics that make it competitive with respect to the state-of-the-art. For instance, a chaos-OTDR able to achieve similar (centimeter) resolution in long distance measurements has been demonstrated [28], with monitoring times as low as 2 ms. However, the technique is limited to identifying reflective events in a fiber. It is important to highlight that, even though used in a different context in [28], filtered broadband sources are not indicated for the measurements presented in Fig. 7 and 8. The fact that the demonstrated spatial resolution can be maintained for long-distance measurements is only possible due to the tunable F8-PMLL, which creates short-pulses with a relatively narrow spectral bandwidth. This way, chromatic dispersion does not severely limit the spatial resolution as more distant positions of the fiber are probed. In e.g. [29], a filtered broad band source was used to perform centimeter resolution measurements and a study of the impact of the chromatic dispersion (as the spectral bandwidth of the filter was varied) in the achievable spatial resolution was performed.

## IV. Conclusion

By combining the time resolution of a TDC with the management capabilities of an FPGA, a detection system could be developed that allows for high resolution measurements with high data acquisition rates. This structure, when employed together with an optical pulse generation system that allows for wavelength tunability and high-peak-power narrow pulses culminates into the fast acquisition tunable high-resolution photon-counting OTDR, with an achievable spatial resolution of 4.6 cm and 15 dB dynamic range. The current bottleneck of the system is the throughput of the TDC, that handles a limited amount of detection events. Improving the TDC's data handling capacity, narrowing the pulse width of the F8-PMLL, and migrating the detection system in order to make use of superconducting nanowire single-photon detectors are the main future points of investigation, which have the potential to lead to sub-centimeter spatial resolution with an even higher achievable dynamic range. The realization of a system where a single optical pulse can be used to monitor distinct positions of a fiber in a high-resolution photon-counting OTDR enables dramatic gains in acquisition time and, in turn, full long-distance fiber measurements with centimeter resolution.

## Acknowledgment

The authors acknowledge the financial support from brazilian agencies CAPES, CNPq, and FAPERJ.

## References

[1] S. Kumar and M. J. Deen, *Fiber optic communications: fundamentals and applications*. John Wiley & Sons, 2014.

[2] P. J. Urban, G. Vall-Llosera, E. Medeiros, and S. Dahlfort, "Fiber plant manager: An otdr-and otm-based pon monitoring system," *IEEE Communications Magazine*, vol. 51, no. 2, pp. S9–S15, 2013.

[3] K. O. Hill and G. Meltz, "Fiber bragg grating technology fundamentals and overview," *Journal of lightwave technology*, vol. 15, no. 8, pp. 1263–1276, 1997.

[4] M. Barnoski, M. Rourke, S. Jensen, and R. Melville, "Optical time domain reflectometer," *Applied optics*, vol. 16, no. 9, pp. 2375–2379, 1977.

[5] G. P. Agrawal, *Fiber-optic communication systems*. John Wiley & Sons, 2012, vol. 222.

[6] G. C. Amaral, L. E. Herrera, D. Vitoreti, G. P. Temporão, P. J. Urban, and J. P. von der Weid, "Wdm-pon monitoring with tunable photon counting otdr," *IEEE Photonics Technology Letters*, vol. 26, no. 13, pp. 1279–1282, 2014.

[7] L. Herrera, F. Calliari, J. Garcia, G. Amaral, and J. von der Weid, "High resolution automatic fault detection in a fiber optic link via photon counting otdr," in *Optical Fiber Communication Conference*. Optical Society of America, 2016, pp. M3F–4.

[8] G. C. Amaral, J. D. Garcia, L. E. Herrera, G. P. Temporao, P. J. Urban, and J. P. von der Weid, "Automatic fault detection in wdm-pon with tunable photon counting otdr," *Journal of Lightwave Technology*, vol. 33, no. 24, pp. 5025–5031, 2015.

[9] F. Calliari, L. E. Herrera, J. P. von der Weid, and G. C. Amaral, "High-dynamic and high-resolution automatic photon counting otdr for optical fiber network monitoring," in *Proceedings of the 6th International Conference on Photonics, Optics and Laser Technology*, vol. 1, 2018, pp. 82–90.

[10] M. Wegmuller, J. Von Der Weid, P. Oberson, and N. Gisin, "High resolution fiber distributed measurements with coherent ofdr," in *Proc. ECOC 2000*, vol. 11, no. 4. Munich, Germany, 2000, p. 109.

[11] J. P. von der Weid, M. H. Souto, J. D. Garcia, and G. C. Amaral, "Adaptive filter for automatic identification of multiple faults in a noisy otdr profile," *Journal of Lightwave Technology*, vol. 34, no. 14, pp. 3418–3424, 2016.

[12] M. Lunglmayr and G. C. Amaral, "Linearized bregman iterations for automatic optical fiber fault analysis," *IEEE Transactions on Instrumentation and Measurement*, vol. 68, no. 10, pp. 3699–3711, 2018.

[13] M. Salhi, F. Amrani, H. Leblond, and F. Sanchez, "Analytical investigation of a figure-eight single-pulse all-fiber laser based on a nonlinear amplifying loop mirror," *Physical Review A*, vol. 82, no. 4, p. 043834, 2010.

[14] H.-G. Weber and M. Nakazawa, *Ultrahigh-speed optical transmission technology*. Springer Science & Business Media, 2007, vol. 3.

[15] A. Komarov, H. Leblond, and F. Sanchez, "Passive harmonic mode-locking in a fiber laser with nonlinear polarization rotation," *Optics communications*, vol. 267, no. 1, pp. 162–169, 2006.

[16] Y. Chen, F. Kärtner, U. Morgner, S. Cho, H. Haus, E. Ippen, and J. Fujimoto, "Dispersion-managed mode locking," *JOSA B*, vol. 16, no. 11, 1999.

[17] M. E. Fermann, F. Haberl, M. Hofer, and H. Hochreiter, "Nonlinear amplifying loop mirror," *Optics Letters*, vol. 15, no. 13, pp. 752–754, 1990.

[18] I. N. Duling, "All-fiber ring soliton laser mode locked with a nonlinear mirror," *Optics letters*, vol. 16, no. 8, pp. 539–541, 1991.

[19] M. Kues, C. Reimer, B. Wetzel, P. Roztocki, B. E. Little, S. T. Chu, T. Hansson, E. A. Viktorov, D. J. Moss, and R. Morandotti, "Passively mode-locked laser with an ultra-narrow spectral width," *Nature Photonics*, vol. 11, no. 3, p. 159, 2017.

[20] H.-R. Chen, K.-H. Lin, C.-Y. Tsai, H.-H. Wu, C.-H. Wu, C.-H. Chen, Y.-C. Chi, G.-R. Lin, and W.-F. Hsieh, "12 ghz passive harmonic mode-locking in a 1.06 $\mu$m semiconductor optical amplifier-based fiber laser with figure-eight cavity configuration," *Optics letters*, vol. 38, no. 6, pp. 845–847, 2013.

[21] D. Derickson, C. Hentschel, and J. Vobis, *Fiber optic test and measurement*. Prentice Hall PTR New Jersey, 1998, vol. 8.

[22] S. Cova, M. Ghioni, A. Lotito, I. Rech, and F. Zappa, "Evolution and prospects for single-photon avalanche diodes and quenching circuits," *journal of modern optics*, vol. 51, no. 9-10, pp. 1267–1288, 2004.

[23] S. Cova, A. Lacaita, and G. Ripamonti, "Trapping phenomena in avalanche photodiodes on nanosecond scale," *IEEE Electron device letters*, vol. 12, no. 12, pp. 685–687, 1991.

[24] D. A. Miller, "Optical interconnects to silicon," *IEEE Journal of Selected Topics in Quantum Electronics*, vol. 6, no. 6, pp. 1312–1317, 2000.

[25] B. Li, Q. Zhou, H. Zhou, Y. Wang, G. Deng, Y. Wang, H. Li, R. Zhang, K. Qiu, and H. Song, "850nm gain-switched pulse laser and its application in photon counting otdr," in *Optical Metrology and Inspection for Industrial Applications V*, vol. 10819. International Society for Optics and Photonics, 2018, p. 1081915.

[26] J. Hu, Q. Zhao, X. Zhang, L. Zhang, X. Zhao, L. Kang, and P. Wu, "Photon-Counting Optical Time-Domain Reflectometry Using a Superconducting Nanowire Single-Photon Detector," *Journal of Lightwave Technology*, vol. 30, no. 16, pp. 2583–2588, 2012.

[27] P. Eraerds, M. Legré, J. Zhang, H. Zbinden, and N. Gisin, "Photon Counting OTDR: Advantages and Limitations," *Journal of Lightwave Technology*, vol. 28, no. 6, pp. 952–964, 2010.

[28] Z. Wang, M. Fan, L. Zhang, H. Wu, D. Churkin, Y. Li, X. Qian, and Y. Rao, "Long-range and high-precision correlation optical time-domain reflectometry utilizing an all-fiber chaotic source," *Optics Express*, vol. 23, no. 12, pp. 15 514–15 520, 2015.

[29] L. E. Ynoquio Herrera, G. C. Amaral, and J. P. von der Weid, "Remote fiber bragg grating-based sensor characterization with ultra-high-resolution tunable photon counting otdr," in *2017 SBMO/IEEE MTT-S International Microwave and Optoelectronics Conference (IMOC)*, 2017, pp. 1–4.